The Astrophysical Journal Letters, 886:L24 (6pp), 2019 December 1 https://doi.org/10.3847/2041-8213/ab564d
© 2019. The American Astronomical Society. All rights reserved.

First Results from *TESS* Observations of Comet 46P/Wirtanen

Tony L. Farnham, Michael S. P. Kelley, Matthew M. Knight, and Lori M. Feaga
University of Maryland, Department of Astronomy, College Park, MD 20742, USA; farnham@astro.umd.edu
Received 2019 August 27; revised 2019 October 31; accepted 2019 November 12; published 2019 November 22

Abstract

We report on initial results from 20 days' worth of *Transiting Exoplanet Survey Satellite* spacecraft observations of comet 46P/Wirtanen. The long-duration, high-cadence measurements show a 2018 September 26 outburst that exhibited a two-phase, 0.5 mag brightening profile, and may be the best temporally characterized natural outburst ever recorded. Gas velocities from the outburst peaked at 800 m s^{-1}, while dust expanded at only 10s of m s^{-1}. Coadded images also revealed a previously unreported dust trail that extends beyond the 24° field of view.

Unified Astronomy Thesaurus concepts: Comets (280); Short period comets (1452)

1. Introduction

The *Transiting Exoplanet Survey Satellite* (*TESS*) searches for extrasolar planets by observing a sector of the sky for 27.4 days and using high-quality photometric measurements of the stars in the field to look for transits (Ricker et al. 2015). A *TESS* sector covers 84° of ecliptic latitude ($|\beta| > 6°$) with four cameras, each with a 24° field of view (21″ pixels). Images are obtained every 2 minutes and then coadded into 30 minute exposures that are saved as full-frame images (FFIs). During its 27.4 day window, each sector may produce as many as 1315 observations. *TESS* will observe 26 of these sectors (13 south and 13 north of the ecliptic plane) covering 90% of the sky during its 2 yr primary mission.

Because of the large field of view, comets and asteroids serendipitously appear in the *TESS* data. Approximately 50 comets will be bright enough to be detected in the two years of *TESS* observations, and we are using the long-duration, high-cadence observations to monitor these comets for rotational variability, outburst activity, and coma studies. The data are ideal for exploring lightcurve behavior, because the 30 minute cadence permits studies of short-term variability, while the 27 day sequences allow measurements of periodicities >24 hr (which are difficult to obtain from ground-based observations) and provide the opportunity to search for changes in the rotation rate (e.g., Bodewits et al. 2018). The *TESS* observations are also well-suited for outburst studies, as the continuous coverage and high-precision photometric capabilities allow searches for even small events. For any outbursts that occur during a 27 day sector window, the 30 minute cadence will accurately document the start-time, brightening profile, and peak brightness—characteristics that are rarely captured for typical outburst detections—allowing for detailed comparisons that could provide clues to the mechanisms at work in this phenomenon. Finally, the wealth of observations allow for studies of the spatial structures in cometary comae, including the ability to coadd large amounts of data (phased to rotation periods if they are known) to investigate faint features that might exist.

In its approach to perihelion, comet 46P/Wirtanen appeared within the *TESS* field of view. Wirtanen is a particularly interesting comet for demonstrating *TESS*'s potential contributions to cometary science. It is a small hyperactive comet that made an historically close approach to the Earth (0.077 au) in 2018 December, and is a potential target for future spacecraft missions. We report here on first results from the observations of a comet with *TESS*.

2. *TESS* Observations

During the 2018 *TESS* Sector 3 observations, Wirtanen appeared in the field of view of Camera 2, CCD #3. From September 20 to October 17, 1288 FFI images of the comet were acquired. During this time, the comet's heliocentric distance dropped from 1.51 to 1.30 au and the geocentric distance from 0.58 to 0.36 au, while the solar phase angle changed from 23°.2 to 29°.8. During the first and last three days of the sector observations, the spacecraft was testing new pointing software, increasing the jitter (Fausnaugh et al. 2019) and causing ∼340 observations to be considered "non-science-quality." Other suboptimal images include a sequence in which the scattered light from Earth was not well removed and occasional frames that are smeared due to *TESS* momentum dumps that occur every ∼2.5 days. Although some of these data may be recoverable, we have removed them for the initial analyses reported here. In total, we used 935 images spanning 20.4 days.

3. Data Reduction and Analyses

The FFI data are crowded with stars that must be removed to minimize their interference with measurements of the moving comet and we adopted the *TESS* user-provided Difference Image Analysis software (DIA; Oelkers & Stassun 2018) to perform this task. DIA is designed to highlight objects whose brightnesses vary with time, and as an intermediate step in the reduction procedures the scattered light (from the Earth, Moon, etc.) and background stars are removed from each image. We use these intermediate, cleaned images, an example of which is shown in Figure 1, for our comet analyses. The procedure does a good job removing the fainter stars and the wings of brighter stars, but due to the undersampled point-spread function (PSF; Vanderspek et al. 2018), uncorrelated residuals remain at the centers of bright stars. These residuals can still interfere with the comet photometry, but at a significantly lower level than the stars in the original images.

TESS pipeline products are calibrated to $e^- s^{-1}$, which can be converted to *TESS* magnitudes (15,000 $e^- s^{-1}$ corresponds to $T = 10.0$; Vanderspek et al. 2018). Using the Web *TESS*

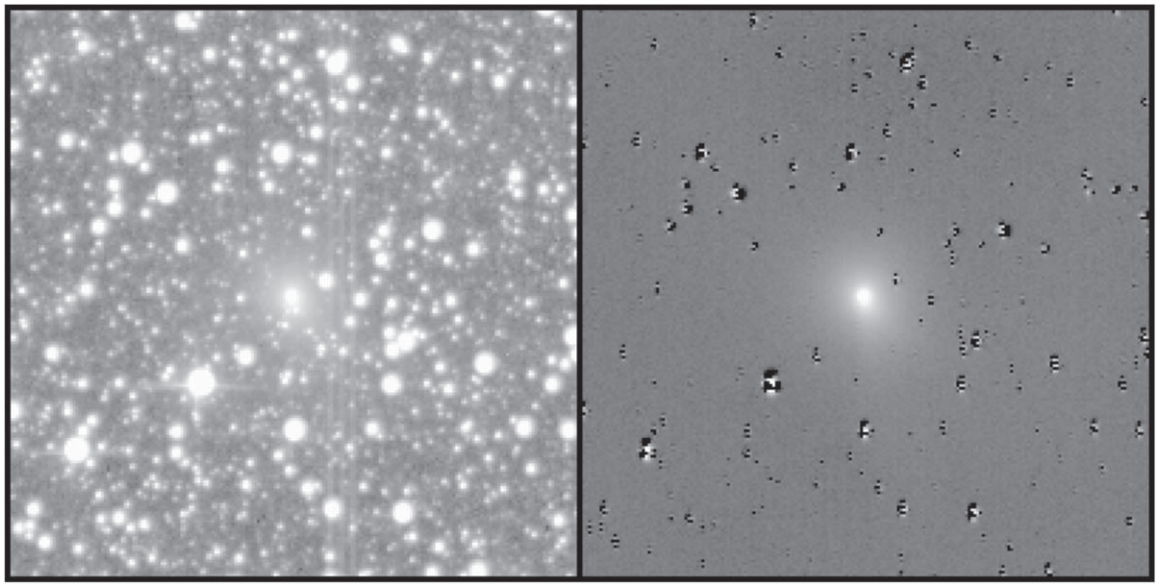

Figure 1. Example of the star and background removal, showing the region of a sample frame (tess2018284152940-s0003-2-3-0123-s_ffic_sa) surrounding comet Wirtanen before (left) and after (right) the DIA cleaning process. The images are 1.22×10^6 km across and are displayed with the same logarithmic scale.

Viewing Tool,[1] which requires an object's brightness in multiple bandpasses (we used typical comet colors $V - J = 1.47 \pm 0.17$ and $J - H = 0.52 \pm 0.12$, Hartmann et al. 1982; and $V - R = 0.50 \pm 0.03$, Jewitt 2015), we produced a rough conversion to R magnitudes,. The systematic uncertainty in R is dominated by the uncertainties in the comet colors, with a conservative estimate of ± 0.3 mag. Relative photometry from image to image, on the other hand, is more tightly constrained, with errors <0.017 mag. Flux units are computed using the conversion coefficient for an $R = 0$ star of 2.18×10^8 W m^{-2} μ m^{-1} (Bessell et al. 1998).

3.1. Lightcurve and Outburst

Centering on the optocenter of the coma, we measured the brightness of the comet in multiple apertures with fixed radii ranging from 15,000 to 40,000 km at the distance of the comet. To produce our lightcurve, we ultimately selected the 25,000 km aperture, which is large enough to contain at least three PSFs at all comet distances, but minimizes the number of residual stars crossing the aperture. The resulting lightcurve, shown in Figure 2, shows the comet continuously brightening over the observation window, but more importantly, it reveals that *TESS* captured a moderate-sized (0.5 mag) outburst—the only one to be reported during the 2018 apparition. This event is likely to be the best temporally characterized natural outburst ever recorded, with the nominal pre-outburst behavior, the onset and rise to the peak, and ultimately the falloff over the course of several weeks, all being observed at a 30 minute cadence. The observations show a two-phase brightening, with a rapid $\sim$1 hr jump commencing on September 26.12 $\pm$ 0.01, followed by a more gradual increase that continued for another $\sim$8 hr. After peaking, the coma began a roughly exponential fading that lasted 15–20 days. Because the comet's pre-outburst brightening rate is not well constrained, it is not clear whether or not the comet had returned to its baseline level by the end of the observation window.

[1] https://heasarc.gsfc.nasa.gov/cgi-bin/tess/webtess/wtv.py

Following up on this discovery, we inspected the images for additional information about the outburst. We registered and coadded the data in 3 hr blocks to improve the signal-to-noise ratio, and then enhanced the post-outburst images by dividing out a pre-outburst frame. The resulting sequence (e.g., Figure 3) shows the rapid brightening of the central coma, followed by an outflow of material that is roughly symmetric around the nucleus. The leading edge of this outflow had a projected velocity $\sim$800 m s^{-1}, suggesting that it was gas related to, and possibly driving, the outburst. Given the detector bandpass (600–1000 nm) the gas was most likely dominated by CN, with emission bands at 914.1 and 787.3 nm (Schleicher 1983). The gas contributes only a few percent of the total brightness within the aperture.

In images over the few days following the outburst, the rapidly moving gas diffuses away, while, in contrast, the bright central peak (presumably dust) remained highly concentrated, showing little radial expansion over the following 15–20 days. This material left our photometric aperture primarily when it dispersed down the tail under the influence of radiation pressure (see Figure 4). Thus, the optically dominant grains ejected in this event must have been moving slowly, with expansion velocities of a few tens of m s^{-1} (consistent with those seen in outbursts in comet 49P/Arend–Rigaux and 67P/Churyumov–Gerasimenko; Eisner et al. 2017; Lin et al. 2017), or else they would have left the photometric aperture more rapidly than was observed.

3.2. Dust Trail

Examination of the *TESS* images also revealed that Wirtanen has a previously unreported dust trail. Due to the presence of the comet itself, the DIA software oversubtracts the background in the vicinity of the coma and trail. To better investigate the trail, we grouped images into 5 day bins, reprojected the raw frames into the comet's rest frame with the velocity vector aligned, masked the bright stars, and then combined the images via the median value at each pixel. The resultant images were additionally filtered to remove the CCD banding artifacts. A sample mosaic is presented in Figure 5.

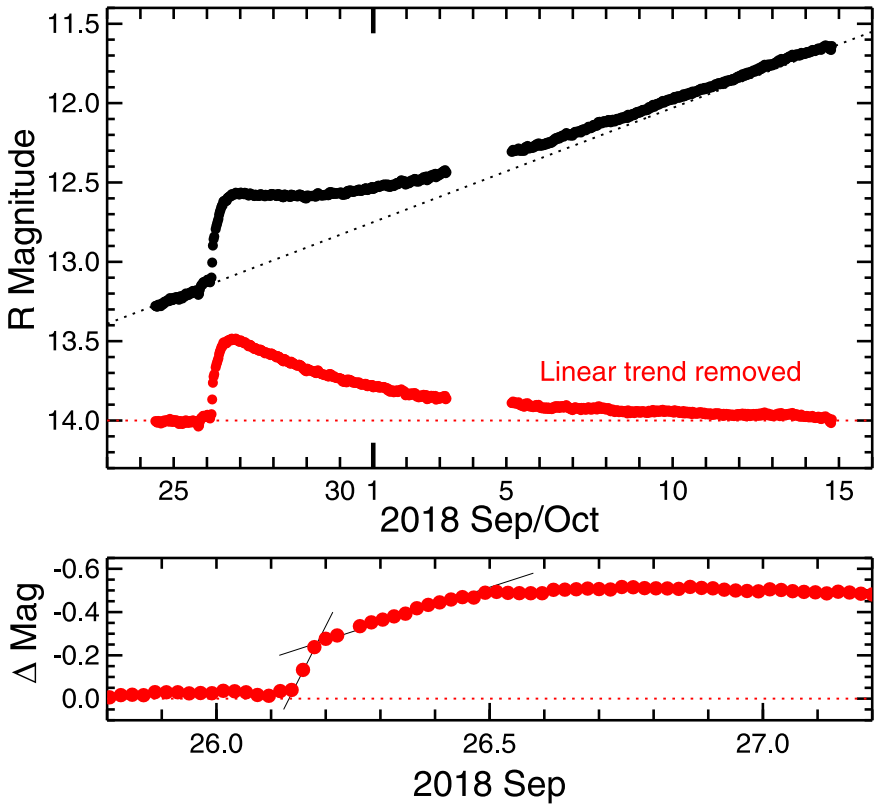

Figure 2. Comet Wirtanen's lightcurve as measured in a 25,000 km radius aperture from the TESS images. The top panel shows the comet's secular brightening (black points) and reveals an outburst that begins at September 26.12. Removing an assumed linear baseline (dotted line) highlights the outburst behavior (red points). The lower panel expands the section around the onset of the outburst, showing the rapid, hour-long jump (0.21 mag hr^{-1}), followed by a more gradual brightening (0.034 mag hr^{-1}) that peaks ~8 hr later. See Section 3 for a discussion of the uncertainties.

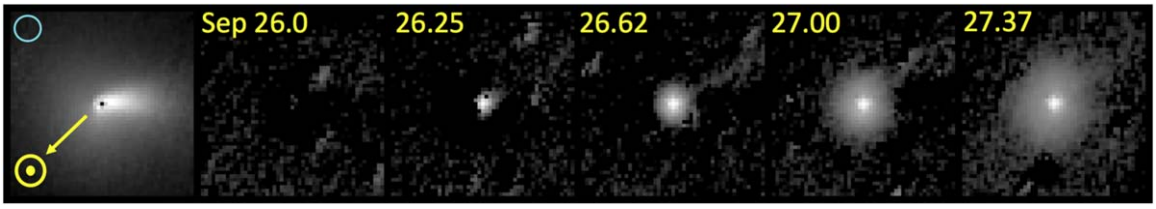

Figure 3. Image sequence showing the outburst's effect on Wirtanen's coma. The first panel shows the pre-outburst morphology, enhanced by dividing out a $1/\rho$ profile. To show changes in the coma with time, panels (2)–(6) are enhanced by subtracting out the (unenhanced) image from panel (1), scaled by the linear trend shown in Figure 2. Panels (2) and (3) bracket the onset of the outburst (September 26.12) and (4)–(6) show the bright central condensation and the rapidly expanding gas cloud. Each panel is 400,000 km across, with north up and east to the left. The light blue circle denotes a 25,000 km radius aperture.

The dust trail extends in both directions beyond the 24° *TESS* field of view, which covers a mean anomaly range (ΔM) of $-1\overset{\circ}{.}6$ to $0\overset{\circ}{.}7$. A Gaussian function fit to the width of the trail at $\Delta M = -0\overset{\circ}{.}16$ ($-1\overset{\circ}{.}7$ on the sky) has a peak of 29.3 mag $arcsec^{-2}$ and a 1σ width of $(5.5 \pm 1) \times 10^4$ km. The width and optical depth ($\tau = 7.0 \times 10^{-12}$) are consistent with the faint end of the range of trails observed at infrared wavelengths (Ishiguro et al. 2009), assuming a 4% geometric albedo.

4. Discussion

Outbursts have been observed in comets for over a century (e.g., Hughes 1990; Filonenko & Churyumov 2006). A number of proposals have been put forth as trigger mechanisms (Hughes 1991; Gronkowski & Wesołowski 2016), though it is generally believed that a single explanation is insufficient to account for all cases. Similarly, little is known about the physical processes that govern the behavior of the ejecta during the initial stages of the event. The main problem is that the majority of outbursts are detected only after they have peaked in intensity and the quasi-exponential fading stage provides few observational constraints on the conditions present during the explosive phase. The excellent coverage of the Wirtanen event allows us to use its characteristics as a baseline model for the behavior of a moderate-sized outburst that can be compared and contrasted with other outbursts. With this information, we can begin exploring the physical processes at work.

4.1. Characterization of Wirtanen's Outburst

To begin this investigation, we can evaluate some potential trigger mechanisms by looking at a comet's history. Wirtanen is not known for exhibiting outburst activity, and only three previous events were reported since its 1948 discovery: 1991 October 7 (+16 days from perihelion, <1 mag; Kronk et al. 2017);

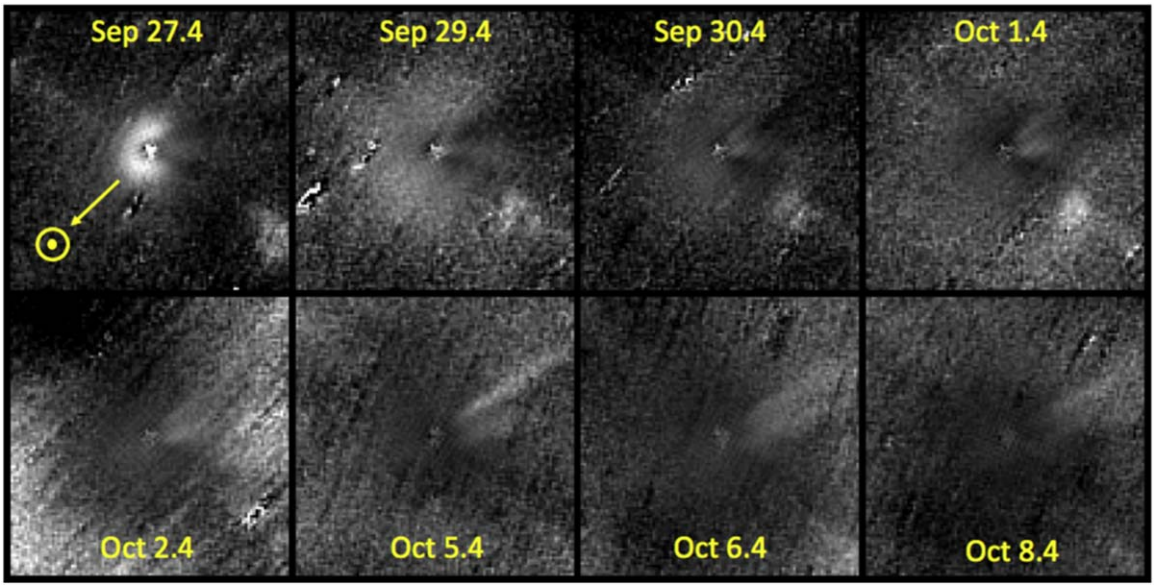

Figure 4. Image sequence showing the effects of Wirtanen's outburst on its dust tail. The first panel highlights the outburst, followed by images that show a narrow tail forming in the antisolar direction over subsequent days. Each panel consists of 8 hr worth of images, centered on the stated date and rotated to align the sunward direction with that of the September 27 panel before coadding. Images were enhanced by combining all images between September 28 and October 9 (again rotated to align the sunward direction) into a single temporally averaged template, which was then divided out of each of the eight coadded panels. Images are 100 pixels across, which ranges from 780,000 km on September 27 to 640,000 km on October 8.

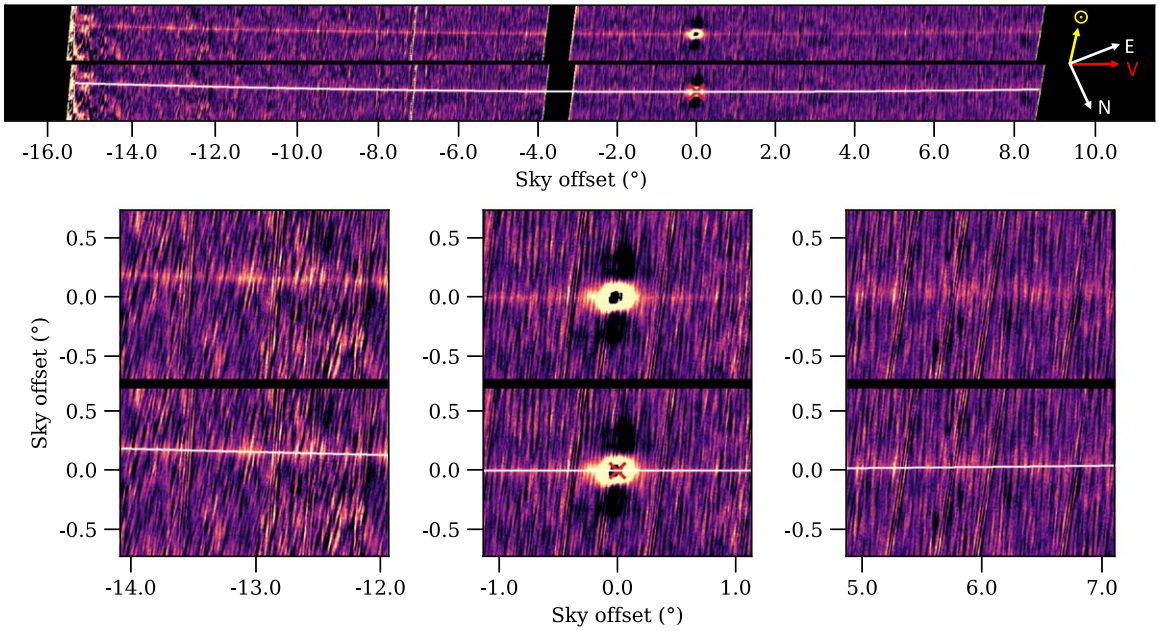

Figure 5. Sample mosaic showing Wirtanen's dust trail, produced by combining 240 images from the 5 day period from September 28 to October 3. The top panel shows the full mosaic, spanning CCDs 3 and 4 in Camera 2; sections at the nucleus and outer ends are expanded below. In the lower frame of each image pair, a cross is located at the nucleus's position and the comet's orbit is overlain, showing that the trail is centered on the comet's path. The direction arrows in the inset are shown for the nucleus's position at the midtime of the 5 day window.

2002 September 25 (+29 days, ~2 mag; Yoshida 2003; Kidger 2004); and 2008 May 16 (+86 days, 2 mag; Kidger 2008). Including the 2018 outburst on September 26 (–81 days), there is no correlation in the orbital position for these outbursts. Furthermore, given the similar viewing geometry on alternate apparitions, there are often observations from ~11 yr before or after the observed outbursts that rule out any events occurring at those points on other orbits. Thus, the lack of correlation between outbursts and the comet's true anomaly or heliocentric distance, combined with the general rarity of these events, suggests that a persistently volatile region, as described by Miles (2016), is not the cause of the Wirtanen events.

Next, we can characterize the scale of the event to provide context for comparisons to other events. The outburst produced a 0.5 mag brightness increase. For a more quantitative measurement, we convert this brightening to an increase in reflective surface area, and then to a mass of the ejected material. We use the photometric analysis outlined by Jewitt (1991), and assume that the brightness increase is dominated by sunlight reflected off dust grains ejected into the coma. For an

initial brightness $R = 13.1$ and a total brightening of 0.5 mag, we find an increase in the optical cross section of $\sim 2 \times 10^8$ m^2 (using the geometric parameters at the start of the outburst, the Halley-Marcus composite dust phase function compiled by D. Schleicher,[2] and an assumed 4% albedo).

Adopting a grain population with density 2000 kg m^{-3}, radii ranging from 0.1 μm to 1 mm and a differential size distribution with a power-law index of -3.5, we find that the above cross section converts to a total dust mass of $\sim 3 \times 10^6$ kg. Unfortunately, the mass tends to be dominated by the largest particles and the dust properties in the outburst are not well constrained, so changing the assumed upper limit of the grain size and/or the power-law index can alter the computed mass by as much as two orders of magnitude for plausible populations. Thus, our best estimate is that the outburst likely produced 10^5–10^8 kg of material. This is equivalent to a crater a few tens of meters in radius (for a bulk nucleus density of 500 kg m^{-3}), which is consistent with the outburst-associated features seen on comet 9P/Tempel 1 (Belton et al. 2008). Pits known to be associated with outbursts are also seen on comet 67P/Churyumov–Gerasimenko (Vincent et al. 2019). Although these features are smaller (<10 m) than that computed for Wirtanen, the related 67P/Churyumov–Gerasimenko outbursts were also smaller, and were not detected from Earth.

An important factor in the Wirtanen outburst is that it is one of the first outbursts whose rise in intensity is well documented, showing a two-phase increase in brightening. Given that the gas was measured to expand outward at $\sim$800 m s^{-1}, while the dust exhibited significantly lower speeds, we know that during the first eight hours following the initiation of the outburst, even the leading edge of the gas cloud would not have escaped our 25,000 km aperture. This means that the two-phase brightness profile must reflect temporal characteristics of the outburst (e.g., the changes in slope are not due to material leaving the aperture). We suggest that the initial, hour-long period of brightening represents the energetic phase in which gas and dust were rapidly ejected into the coma. The second, more gradual phase of brightening is probably due to the continued expansion of the dust from an initially dense state to an optically thin regime. However, it is also possible that this phase arises from other causes: a continued excavation, at a much slower rate as the outburst subsides; temporary enhanced emission of gas and dust produced by sublimation of newly exposed ices; or the increase in reflective surface area as a small number of grains in the coma gradually fragment into smaller particles.

4.2. Comparison to Other Outbursts

Our literature search revealed only three other occasions in which high-cadence coverage was obtained of the brightening phase of an outburst: a 2017 event in 29P/Schwassmann–Wachmann 1 (SW1), the 2007 outburst of comet 17P/Holmes, and the Deep Impact (DI) experiment in comet Tempel 1 in 2005. As discussed below, there are significant differences in the basic nature of each of these events, but we can compare and contrast the observed behavior in the early stages of each case, to explore whether similar mechanisms may be at work.

SW1 is known for frequent outbursts. About half seem to be periodic (Miles et al. 2016), suggesting that the nucleus has volatile-rich hot spots that are triggered by diurnal heating cycles. On 2017 July 2, SW1 experienced a $\sim$2 mag outburst and Miles et al. (2018) reported on high-cadence photometry of this event. Few results from these measurements have been reported, but if we adopt the same assumptions as used in the Wirtanen estimate above, we compute an increase in the SW1 optical cross section of $\sim 10^{11}$ m^2. Because conditions are dramatically different in the two comets, this is likely a poor comparison, but it suggests that the SW1 outburst was significantly larger than that seen in Wirtanen. Even so, the behavior of the lightcurve during the initial stages appears to be nearly identical in character to the Wirtanen event, with a rapid rise for $\sim$0.5 hr, followed by a more gradual increase that continued for at least another hour, when the observations ended. The fact that both events exhibit similar behavior, even in their timescales, suggests that the physical mechanisms governing the ejecta are the same, even though the magnitude of the events were dramatically different.

Comet Holmes experienced a 15 mag brightening—the largest outburst ever recorded—around 2007 October 23.7 (Montalto et al. 2008; Stevenson & Jewitt 2012). The onset of the outburst was not captured, but the 42 hr duration of the rise allowed observers to capture the later stages of the brightness increase (Trigo-Rodriguez et al. 2008; Hsieh et al. 2010; Li et al. 2011). This lightcurve shows that there was a change in the rate of brightening around October 24.1, around half a day into the outburst, where the rate became *steeper*, before inflecting and then peaking a day later. This steepening in slope was shown to be the result of a rapid cascade of large dust grains fragmenting into successively smaller particles, which dramatically increased the reflective surface area in the coma (Hsieh et al. 2010; Stevenson & Jewitt 2012). In the days following the outburst, the leading edge of the ejected dust cloud was measured to have a velocity $\sim$550 m s^{-1} (e.g., Trigo-Rodriguez et al. 2008), an order of magnitude higher than the dust velocities in Wirtanen, which likely reflects the enormous amount of energy released in the event.

Our final comparative example is the DI experiment at comet Tempel 1 (T1). Although this was a man-made outburst, it was known to be the result of an impact and should exhibit the same phenomena as a naturally triggered impact event. Furthermore, because it was planned, it was intensely observed from both DI and from the ground, allowing remote observations to be connected to specific events seen by the spacecraft. High-cadence photometry of the event shows a three-phase brightening (Meech et al. 2005; Fernández et al. 2007; Küppers et al. 2009; Mitchell et al. 2010). The T1 lightcurve starts with a very sharp increase for the first $\sim$1 minutes, followed by 6 minutes of gradual brightening, and then another 10–15 minutes with a somewhat steeper slope before it flattened out at $\sim$2 mag above its starting brightness. The first two phases mimic the behavior of Wirtanen and SW1, while the later steepening is comparable to that seen in Holmes. The outburst started to fade $\sim$45 minutes after impact. The peak velocity of the ejecta was $\sim$200 m s^{-1}. It is interesting to note that details in the observed phenomena, including changes in the brightness slope, peak intensity, and timing of the observed features, vary somewhat depending on the aperture size, wavelength, etc., and exploring these differences should provide additional information for exploring the behavior of the ejecta.

As was suggested in Section 4.1 the two-phase brightness increase is related to the initial ejection of highly dense material that then becomes optically thin as it expands outward. The T1 data provide a test of this conjecture. Kolokolova et al. (2016) used DI observations of the ejecta in front of the comet's limb

[2] https://asteroid.lowell.edu/comet/dustphase.html

to measure the optical thickness of the dust. They found that the cloud started out optically thick, but tended to thin within a few seconds in most areas. However, a few bands of material remained optically thick for as long as a minute. This time frame corresponds to that of the steep segment of the photometric profile, suggesting that the change in slope may indeed be due to the expansion of the ejecta into an optically thin regime. The difference in timescales between Wirtanen and T1 are likely to be due to differences in velocity as well as the properties of the ejecta.

The comparisons between the initial stages of these four outbursts reveal both similarities and differences. The similarities suggest that common processes govern the physics, regardless of the cause or size of the event, while the differences, such as the shorter timescale seen in T1 or the long duration of the Holmes brightness increase, could represent characteristic signatures that provide clues to the mechanisms involved. Results for comet Wirtanen also show the promise that *TESS* observations hold for cometary science.

This Letter includes data collected by the *TESS* mission, which are publicly available from the Mikulski Archive for Space Telescopes (MAST). Funding for the *TESS* mission is provided by NASA's Science Mission directorate.

Facility: TESS.

Software: DIA (Oelkers et al. 2015; Oelkers & Stassun 2018), Astropy (Astropy Collaboration et al. 2013, 2018), SEP (Barbary 2016).

ORCID iDs

Tony L. Farnham https://orcid.org/0000-0002-4767-9861
Michael S. P. Kelley https://orcid.org/0000-0002-6702-7676
Matthew M. Knight https://orcid.org/0000-0003-2781-6897
Lori M. Feaga https://orcid.org/0000-0002-4230-6759

References

Astropy Collaboration, Price-Whelan, A. M., Sipőcz, B. M., et al. 2018, AJ, 156, 123
Astropy Collaboration, Robitaille, T. P., Tollerud, E. J., et al. 2013, A&A, 558, A33
Barbary, K. 2016, JOSS, 1, 58
Belton, M. J. S., Feldman, P. D., A'Hearn, M. F., & Carcich, B. 2008, Icar, 198, 189
Bessell, M. S., Castelli, F., & Plez, B. 1998, A&A, 333, 231
Bodewits, D., Farnham, T. L., Kelley, M. S. P., & Knight, M. M. 2018, Natur, 553, 186
Eisner, N., Knight, M. M., & Schleicher, D. G. 2017, AJ, 154, 196
Fausnaugh, M. M., Caldwell, D. A., & Jenkins, J. M. 2019, TESS Data Release Notes: Sector 3, DR4, NASA/TM-2018-220181, https://archive.stsci.edu/missions/tess/doc/tess_drn/tess_sector_03_drn04_v02.pdf
Fernández, Y. R., Lisse, C. M., Kelley, M. S., et al. 2007, Icar, 187, 220
Filonenko, V. S., & Churyumov, K. I. 2006, AdSpR, 38, 1940
Gronkowski, P., & Wesołowski, M. 2016, EM&P, 119, 23
Hartmann, W. K., Cruikshank, D. P., & Degewij, J. 1982, Icar, 52, 377
Hsieh, H. H., Fitzsimmons, A., Joshi, Y., Christian, D., & Pollacco, D. L. 2010, MNRAS, 407, 1784
Hughes, D. W. 1990, QJRAS, 31, 69
Hughes, D. W. 1991, in IAU Colloq. 116, Comets in the post-Halley era ed. R. L. J. Newburn, M. Neugebauer, & J. Rahe (Dordrecht: Kluwer Academic), 825
Ishiguro, M., Sarugaku, Y., Nishihara, S., et al. 2009, AdSpR, 43, 875
Jewitt, D. 1991, in IAU Coll. 116, Comets in the Post-Halley era ed. R. L. J. Newburn, M. Neugebauer, & J. Rahe (Dordrecht: Kluwer Academic), 19
Jewitt, D. 2015, AJ, 150, 201
Kidger, M. 2008, Astron. Electron. Circ. 2446, http://www.theastronomer.org/tacirc/2008/e2446.txt
Kidger, M. R. 2004, A&A, 420, 389
Kolokolova, L., Nagdimunov, L., A'Hearn, M., King, A., & Wolff, M. 2016, P&SS, 133, 76
Kronk, G. W., Meyer, M., & Seargent, D. A. J. 2017, Cometography: A Catalog of Comets, Vol. 6 (Cambridge: Cambridge Univ. Press)
Küppers, M., Keller, H. U., Fornasier, S., et al. 2009, in Deep Impact as a World Observatory Event: Synergies in Space, Time, and Wavelength, ed. H. U. Käufl & C. Sterken (Berlin: Springer), 29
Li, J., Jewitt, D., Clover, J. M., & Jackson, B. V. 2011, ApJ, 728, 31
Lin, Z.-Y., Knollenberg, J., Vincent, J. B., et al. 2017, MNRAS, 469, S731
Meech, K. J., Ageorges, N., A'Hearn, M. F., et al. 2005, Sci, 310, 265
Miles, R. 2016, Icar, 272, 387
Miles, R., Faillace, G. A., Mottola, S., et al. 2016, Icar, 272, 327
Miles, R., Soulier, J.-F., Angel, T., et al. 2018, EPSC, 523
Mitchell, T. R., Welsh, W. F., Etzel, P. B., et al. 2010, Icar, 205, 619
Montalto, M., Riffeser, A., Hopp, U., Wilke, S., & Carraro, G. 2008, A&A, 479, L45
Oelkers, R. J., Macri, L. M., Wang, L., et al. 2015, AJ, 149, 50
Oelkers, R. J., & Stassun, K. G. 2018, AJ, 156, 132
Ricker, G. R., Winn, J. N., Vanderspek, R., et al. 2015, JATIS, 1, 014003
Schleicher, D. G. 1983, PhD thesis, Maryland Univ.
Stevenson, R., & Jewitt, D. 2012, AJ, 144, 138
Trigo-Rodriguez, J. M., Davidsson, B., Montanes-Rodriguez, P., Sanchez, A., & Troughton, B. 2008, LPSC, 39, 1627
Vanderspek, R., Doty, J., Fausnaugh, M. M., et al. 2018, TESS Instrument Handbook, 0.1, Mikulski Archive for Space Telescopes, https://archive.stsci.edu/missions/tess/doc/TESS_Instrument_Handbook_v0.1.pdf
Vincent, J.-B., Farnham, T., Kührt, E., et al. 2019, SSRv, 215, 30
Yoshida, S. 2003, 46P/Wirtanen (2002), 46, http://www.aerith.net/comet/catalog/0046P/2002.html